On Active/Reactive Power Modulation of DFIG-based Wind Generation for Inter-area Oscillation Damping

Lingling Fan, *Senior Member, IEEE*, Haiping Yin, *Student Member, IEEE*, Zhixin Miao, *Senior Member, IEEE*

Abstract—In this paper, the interactions of the torsional dynamics of the wind turbines and power modulation for oscillations in DFIG-based wind generators are investigated. One major concern of active power modulation is its interaction with wind turbine's torsional dynamics. A study case with wind turbine torsional dynamics modeled is derived from [1]. Both active power modulation and reactive power modulation controls are developed in this paper. The paper successfully demonstrates the presence of interaction between active power modulation and torsional dynamics and the absence of such interaction in the case of reactive power modulation. Linear system analysis and root loci approach are employed to demonstrate such interaction. Simulation results in MATLAB/Simulink further verifies the analysis. The major contribution of this paper is: i) the demonstration of the potential disadvantage of wind generation's active power modulation, and ii) the identification of reactive power modulation in wind generation as an alternative for inter-area oscillation damping.

Index Terms—Doubly fed induction generator (DFIG), Inter-area Oscillation Damping, Active Power Modulation, Reactive Power Modulation

NOMENCLATURE

P_m, P_e	mechanical and electrical power
T_m, T_e	mechanical and electromagnetic torques
ω_s, ω_r	stator frequency and rotor rotating speed
r_s, r_r	stator and rotor resistances
L_s, L_r	stator and rotor inductances
M	Mutual inductance between rotor and stator
λ_{qs}, λ_{ds}	q and d axis stator flux linkages
λ_{qr}, λ_{dr}	q and d axis rotor flux linkages
λ_{qm}, λ_{dm}	q and d axis air gap flux linkages
i_{qs}, i_{ds}	q and d axis stator currents
i_{qr}, i_{dr}	q and d axis rotor currents
v_{qs}, v_{ds}	q and d axis stator voltages
v_{qr}, v_{dr}	q and d axis rotor voltages
P_s, Q_s	stator active and reactive power
H_t	Inertia constants for the turbine (s)
H_g	Inertia constants for the generator (s)
D_t	Damping coefficients of the turbine
D_g	Damping coefficients of the generator
D_{tg}	Damping coefficient of the flexible coupling between the two masses
K_{tg}	Shaft stiffness

I. INTRODUCTION

L. Fan, H. Yin and Z. Miao are with Dept. of Electrical Engineering, University of South Florida, Tampa FL 33620. Emails: linglingfan@usf.edu, hyin@mail.usf.edu, and zmiao@usf.edu. Phone: (813)974-2031.

ACtive power modulation has been applied in HVDC to enhance the oscillation stability [2]. Such method has its disadvantage. Active power modulation results in a corresponding change in the generators' electromagnetic torque. Such modulation can interact with the torsional dynamics if the frequencies of electric network oscillations and torsional oscillations are close. This phenomena have been observed in literature [3]. Reactive power modulation to enhance oscillation stability has been used in shunt reactive power compensation devices, such as SVC and STATCOM [4]. In [4], the addition of damping controller was shown to modulate the reference voltage. Since the voltage magnitude is closely related to the reactive power, the addition of damping controller can be thought as reactive power modulation.

Doubly-fed-induction-generator (DFIG)-based wind energy system is the state-of-the-art technology. The advantage of DFIG-based wind generation is its active/reactive power control capability through its rotor side converter (RSC). Considering the high penetration of wind power in future grids, the use of DFIGs to damp oscillations has been discussed in literature [1], [5]–[7].

Power System Stabilizer (PSS) for a wind turbine employing DFIG is given in [5] and the objective there is to damp oscillations. The DFIG control in [5] is based on flux magnitude and angle control (FMAC). An auxiliary damping control is added to modify the flux angle reference, which is obtained from an PI controller to track the active power reference. In [6], an auxiliary signal derived from the rotor speed is added to the rotor phase angle control to enhance the low-frequency damping of the system. The control structure in [6] is derived based on FMAC in [5]. Contribution of DFIG to oscillation damping has been summarized in [7]. Reference [7] points out that active power modulation is a powerful tool to introduce additional damping to interarea oscillations.

While the FMAC for DFIG converters is presented in [5], [6], [8], majority of the control schemes for DFIG including the commercial technology of DFIG are based on stator-voltage oriented vector control [9]–[11]. In vector control scheme, active power control and reactive power control are realized by qd-axis loops. An auxiliary damping control based on vector control scheme is more practical and can be realized for the existing DFIG wind generators.

Active power modulation for interarea oscillation damping has been investigated in [1], in which the active power modulation is shown to be more effective than reactive power modulation using bode plots. However, active power mod-

ulation may interact with the torsional dynamics. In wind turbines, the torsional stiffness and the torsional oscillation frequency are quite low. If active power modulation results in low-frequency oscillations in wind generators, then there is a possibility of these interacting with torsional oscillations. On the other hand, reactive power modulation is immune from the interaction since reactive power is not directly related with the electromagnetic torque. Hence, a preliminary study on reactive power modulation is conducted by the authors in [12]. Active and reactive power modulation methods have been briefly mentioned in [13] without detailed analysis and comparison of the two methods.

This paper presents a thorough analysis of the interaction between power modulation and torsional dynamics. First, the torsional dynamics will be modeled for wind turbines. Both active/reactive power modulation will be compared for their impact on torsional modes. The same study system employed in [1] will be used to study the interaction problem. Compared with [1] where the focus is on the electrical dynamics, this paper presents a bigger picture including both the mechanical dynamics and the power system electrical dynamics.

The remainder of the paper is organized as follows. Section II introduces the model of a DFIG-based wind generator including its control system and power modulation block. Section III presents the study system and its characteristics. Section IV presents the analysis of active/reactive power modulation analysis using root locus and eigenvalue methods. Section V investigates the interaction between the torsional mode and inter-area oscillation mode under active and reactive power modulation methods. Section VI presents the time-domain simulation results which corroborate the analysis in Section V. Section VII concludes the paper.

II. MODEL OF DFIG-BASED WIND GENERATOR

The model of DFIG-based wind generator includes aerodynamics, turbine shaft dynamics, DFIG machine dynamics, DC-link capacitor dynamics, and RSC and GSC control systems. Mei and Pal have pointed out in [14] that DFIGs have a pair of mode related with the stator electromagnetic transient that can be unstable under certain condition, such as improper converter controller parameters. However with reduced order model of DFIG where such transients are ignored, the unstable mode cannot be observed. Mishra and *et al* points out in [6] that for a mode associated with the voltage across the dc-link capacitor can have detrimental effect on the system stability if not properly damped. Therefore, for accurate controller tuning, in this study, the model of DFIG includes the stator transients and the dc capacitor dynamics.

In [1], a single mass model is used to represent the turbine shaft-generator rotor system. The single mass model cannot showcase the turbine shaft mode. In this study, the interaction of active power modulation with the turbine shaft mode is the focus. Hence a two-mass model is adopted for the turbine shaft- generator rotor system.

A. DFIG model

Fig. 1 shows the equivalent circuit of a DFIG in the synchronous qd reference frame, where the q-axis leads the d-axis by 90^0. Stator and rotor voltage equations in qd reference frame can be obtained as follows:

$$\begin{cases} V_s = r_s I_s + j\omega_s \lambda_s + \frac{d\lambda_s}{dt} \\ V_r = r_r I_r + j(\omega_s - \omega_r)\lambda_r + \frac{d\lambda_r}{dt} \end{cases} \quad (1)$$

where $V_s = v_{qs} - jv_{ds}$ and $V_r = v_{qr} - jv_{dr}$. The flux linkage
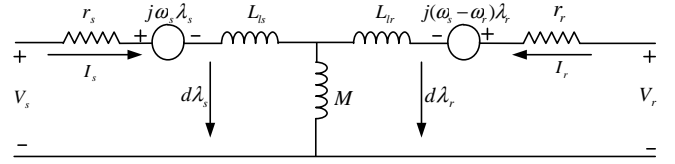

Fig. 1. The equivalent circuit of DFIG.

expressions are given as:

$$\begin{cases} \lambda_s = L_s I_s + M I_r \\ \lambda_r = L_r I_r + M I_s \end{cases} \quad (2)$$

where $L_s = L_{ls} + M$, $L_r = L_{lr} + M$, $\lambda_s = \lambda_{qs} - j\lambda_{ds}$, $\lambda_r = \lambda_{qr} - j\lambda_{dr}$, $I_s = i_{qs} - ji_{ds}$, and $I_r = i_{qr} - ji_{dr}$.

From (1) and (2), a set of differential equations with stator and rotor currents as state variables, stator and rotor voltages as inputs can be established. While the rotor voltages are determined by RSC control scheme, the stator voltages will be determined by the network interface. A detailed modeling approach of DFIGs can be found in [15].

The electromagnetic torque T_e can be expressed as

$$T_e = \lambda_{qm} i_{dr} - \lambda_{dm} i_{qr} \quad (3)$$

where $\lambda_{qm} = \lambda_{qs} - i_{qs}L_{ls}$ and $\lambda_{dm} = \lambda_{ds} - i_{ds}L_{ls}$. λ_{qm} and λ_{dm} are the q-axis and d-axis air gap flux linkages.

B. Wind Turbine Torsional Dynamics Model

A wind generator consists of the generator rotor, turbine shaft, gear box and blade. To take into account both the bending flexibility and the torsional flexibility, a three-mass model is used in [16]. In this paper, a two-mass model is used to represent the wind turbine by only taking into consideration the torsional flexibility. Such a model is also used in several papers [14], [17] when discussing wind turbine mechanical dynamics. The purpose of our study is to capture the torsional dynamics. Using a two-mass model is sufficient in this case to investigate the torsional dynamics we are interested.

The equations of the two-mass model are listed as follows:

$$\begin{cases} 2H_t \frac{d\Delta\omega_t}{dt} = -(D_t + D_{tg})\Delta\omega_t + D_{tg}\Delta\omega_r + T_m - T_{tg} \\ 2H_g \frac{d\Delta\omega_r}{dt} = -(D_t + D_{tg})\Delta\omega_r + D_{tg}\Delta\omega_t + T_{tg} - T_e \\ \frac{dT_{tg}}{dt} = K_{tg}\omega_e(\Delta\omega_t - \Delta\omega_r) \end{cases}$$

$$(4)$$

where D_t and D_g are the damping coefficients of the turbine and generator, D_{tg} is the damping coefficient of the flexible coupling between the two masses, H_t and H_g are the inertia constants for the turbine and the generator, and K_{tg} is the shaft stiffness.
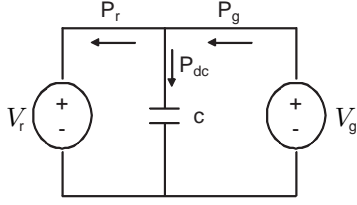
Fig. 2. DC link with V_r and V_g representing RSC and GSC voltage phasors. $V_r = \frac{1}{\sqrt{2}}(v_{qr} - jv_{dr})$, $V_g = \frac{1}{\sqrt{2}}(v_{qg} - jv_{dg})$. v_{qr} and v_{dr} are quadrature axis and direct axis RSC voltages. v_{qg} and v_{dg} are quadrature axis and direct axis GSC voltages.

C. DC link model

The dynamics of the dc link with the capacitor between the rotor and stator side converters are described by a first order model in physical units:

$$Cv_{dc}\frac{dv_{dc}}{dt} = P_r - P_g \tag{5}$$

$$\text{where} \begin{cases} P_r = \frac{1}{2}(v_{qr}i_{qr} + v_{dr}i_{dr}) \\ P_g = \frac{1}{2}(v_{qg}i_{qg} + v_{dg}i_{dg}) \end{cases} \tag{6}$$

P_r and P_g are the active power at RSC and GSC side respectively. Note that all expressions are in physical units.

D. DFIG Converter Controls

Both RSC and GSC controls are modeled in this study. Cascaded control loops similar to those in [14] are adopted in this paper. The control loops are shown in Figs. 3 and 4.
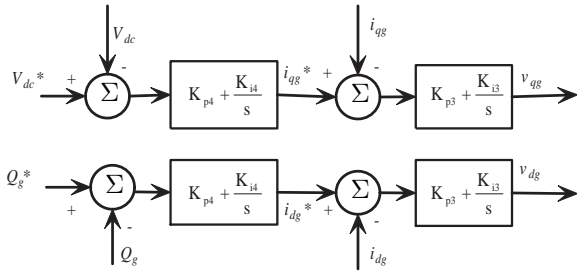
Fig. 3. GSC control loops.

The GSC control loops have two objectives: (a) the q-axis loop is used to keep the dc link voltage constant so the active power through the GSC and RSC will be the same and (b) the d-axis loop is used to regulate the DFIG GSC reactive power Q_g.

The RSC control diagram is shown in Fig. 4 where the reference power is obtained through the maximum power point tracking (MPPT) lookup table. The wind turbine is able to extract maximum wind power from the lookup table. The q-axis loop is used to regulate the active power of the DFIG and the d-axis loop is used to regulate reactive power of the DFIG stator Q_s.

Active power modulation for oscillation stability enhancement has been applied in HVDC [2] while reactive power modulation for oscillation stability has been applied in STATCOM
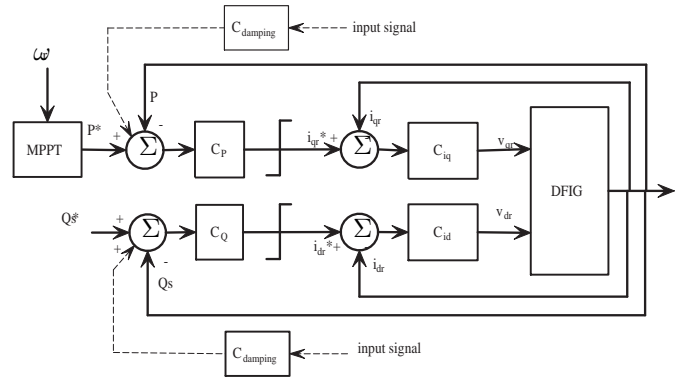

Fig. 4. RSC control loops.

[4]. In Fig. 4, the blocks along the dotted paths are involved in the potential power modulation in a DFIG RSC. The active power modulation will modulate the active power reference value while the reactive power modulation will modulate the reactive power reference value. PI controllers are employed in the control loops such that the measured power (active power or reactive power) tracks the modulated reference power values.
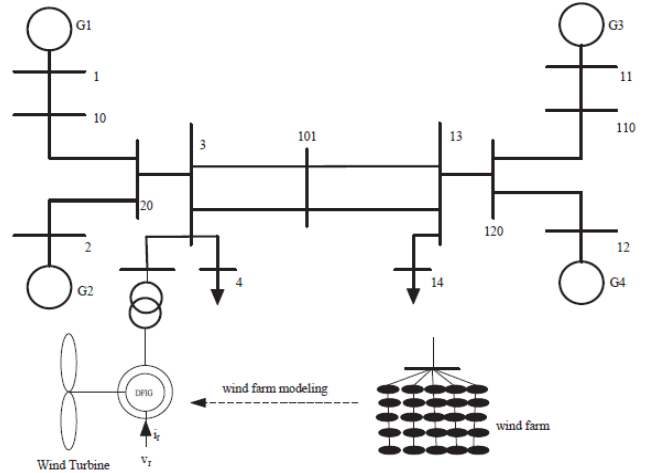
III. THE STUDY SYSTEM

Fig. 5. One-line diagram of a two-area system with a wind generator.

The study system as shown in Fig. 5 is the classic two-area four-machine system. Area 1 has two synchronous generators, each with 835 MW rated power and Area 2 also has two synchronous generators, each with 835 MW rated power. All four synchronous generators are identical and equipped with turbine-governors. The parameters of the synchronous generators [18] are shown in Table I of Appendix along with turbine governor control blocks and parameters. A wind farm based on DFIG is connected to the grid in area one and represented by one aggregated DFIG. The rated exporting level of the wind farm is 200 MW. The parameters of DFIG and wind turbine shaft, RSC and GSC controls are shown in Appendix.

The system has several oscillation modes: i) local electromechanical oscillations (1.2 Hz) due to one synchronous machine swinging against a local area, ii) the inter-area mode (0.75 Hz) due to Area 1 swinging against Area 1, and iii) the wind turbine shaft mode (0.87 Hz). This study system is built in Matlab/Simulink. Generator 1 is equipped with a PSS to increase the damping of its local oscillation. PSS control block and parameters are given in Appendix.

IV. ANALYSIS OF ACTIVE OR REACTIVE POWER MODULATION

It has been suggested and verified in literature that for inter-area oscillation, the best control signal is the rotor angle difference [19], [20]. Hence in this paper, the rotor angle between Gen 3 and Gen 1 (δ_{31}) is selected as the controller input signal or plant output. In the active power modulation method, the plant input is the modulated active power or reactive power as shown in Fig. 4. Active power modulation is first considered.

The detailed model described in Section II is for dynamic simulations. In controller design, linearized models at certain operating condition are first derived from the nonlinear model. The linearization can be done through a function in Matlab called "linmod". The linearized model has an order of 65 and we are facing a large number of system modes. Some of them are not of the interest in this study which focuses on electromechanical dynamics. In order to simplify the linear model, model reduction is used. The reduced model is only used in controller design. When the controller is tested, simulations are conducted based on the detailed model.

The method used for model reduction is the same as that documented in our previous work [1]. The step-by-step procedure is given in [1]. Fast dynamics beyond the interest of electromechanical mode spectrum with adequate damping are ignored. Modes with zeros and poles very close to each other are also eliminated. Hence only few modes are preserved and they are: the local oscillation mode, the inter-area oscillation mode, the shaft mode and the governor mode.

The open-loop system loci of the original system is given in Fig. 6. The root locus diagram of an open-loop system without active power modulation is shown in Fig. 7. Comparison of the two figures gives visual aid to understand which modes are preserved and which modes are ignored. The root loci diagrams in the rest of the section are all based on the reduced-order models.

It is obvious that the system is unstable resulting in inter-area oscillation. With proportional feedback, the damping of the interarea mode will be increased. However, the damping of the shaft mode will be decreased. When the inter-area oscillation has a 5% damping, it is found that the shaft mode will have a negative damping which is desirable. Hence, an improved controller is designed to avoid such a situation. The method of designing the controller is based root locus diagram and it is similar to the one used in [1]. The compensator is designed and the root locus diagram of the open-loop system with the compensator is shown in Fig. 8. It is seen from Fig. 8 that, with an increased gain, the damping for the inter-area oscillation mode increases while that of the shaft mode
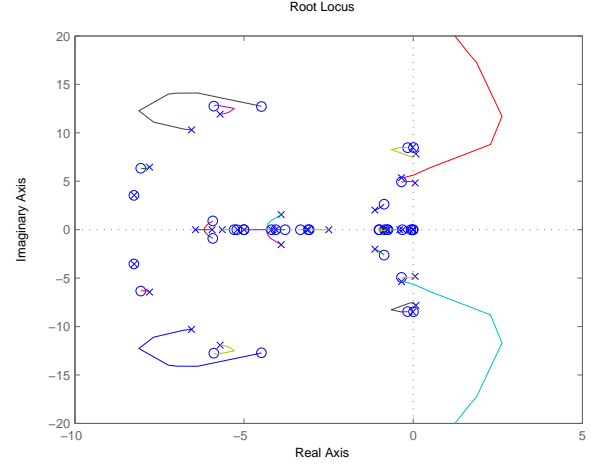

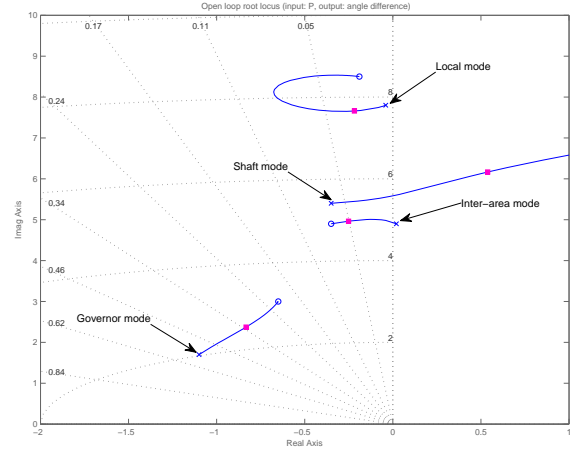Fig. 6. Open-loop system loci without active power modulation based on the original model.

Fig. 7. Open-loop system loci without active power modulation based on the reduced-order model.

decreases. However, the damping of the shaft mode will not be negative. Fig. 8 also demonstrates the interaction between the active power modulation and the shaft mode. It will be undesirable if the damping of the shaft mode becomes too small.

Since the interaction between active power modulation and wind turbine shaft oscillation mode may not yield desired results, reactive power modulation is investigated. The root locus diagram of the open-loop system is shown in Fig. 9 and the open-loop system with a compensator is shown in Fig. 10. In both Figs. 9 and 10, it is found that the shaft mode is not affected at all by an increasing gain. Root locus diagrams show that when reactive power modulation is considered, the zero and the pole corresponding to the shaft mode are located fairly close.

Using the reduced system model, two controllers are designed, one for active power modulation and the other for reactive power modulation. The transfer functions for *active*
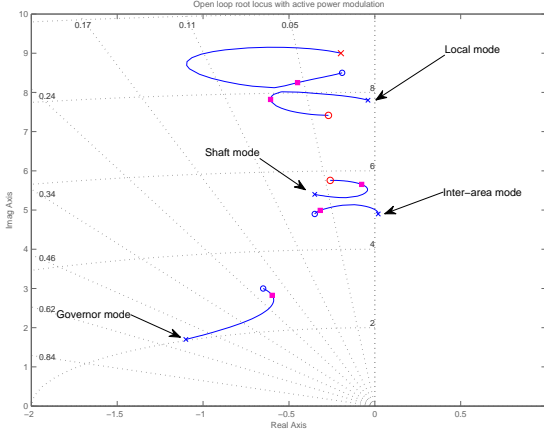
Fig. 8.   Open-loop system root loci with active power modulation.
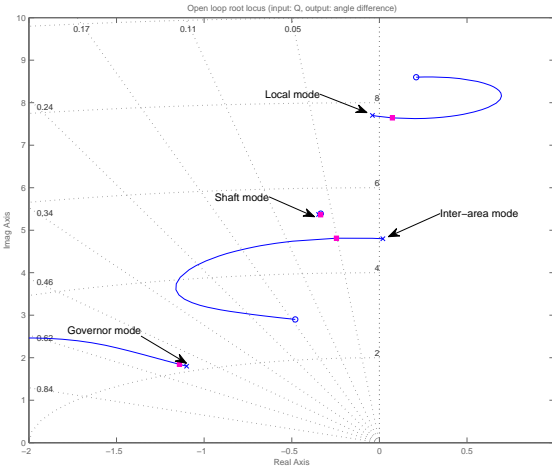

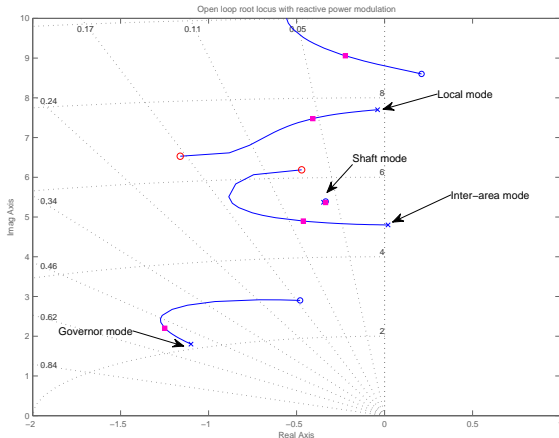Fig. 9.   Open-loop system root loci without reactive power modulation.

Fig. 10.   Open-loop system root loci with reactive power modulation.

power modulation is given by:

$$H(s) = -40 \frac{(0.17^2 s^2 + 0.016s + 1)(0.13^2 s^2 + 0.0098s + 1)}{(0.07s + 1)(0.093s + 1)(0.11^2 s^2 + 0.0049 + 1)}. \tag{7}$$

The transfer function for *reactive power modulation* is given by:

$$H(s) = 98.45 \frac{(0.14^2 s^2 + 0.023s + 1)(0.17^2 + 0.05s + 1)}{(0.12s + 1)(0.21s + 1)(0.09^2 s^2 + 0.0047s + 1)}. \tag{8}$$

It is observed that active power modulation needs a smaller gain than the reactive power modulation. This finding is consistent with the observation in [1] where in bode plots, the gain of the open-loop system of the active power modulation is much high than that of the reactive power modulation. In turn, when the feedback controller is designed to achieve similar performance, a smaller controller gain is required for the system with a high plant gain.

V. SIMULATION RESULTS AND DISCUSSION

Time-domain Simulations are performed on the test system. The power transfer between the two areas is 400 MW. A temporary three-phase fault occurs at Bus 3 at $t = 0s$ and is cleared after 0.1 second. Figs. 11 and 12 show the dynamic responses of the synchronous generators and the DFIG when there is no inter-area oscillation control. In Fig. 11, the relative angle differences, rotor speeds and electric power exporting levels are plotted. In Fig. 12, the rotor speed, mechanical torque, electric torque and terminal voltage of the DFIG are plotted.

The system suffers from low-frequency oscillations. As time goes by, the oscillations increase and the system becomes unstable.
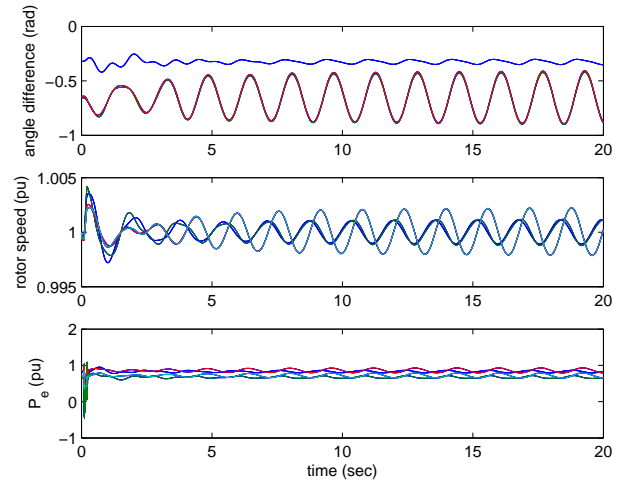

Fig. 11.   Synchronous generator dynamic responses with no supplementary damping control. The first sub-figure shows relative rotor angles δ_{21}, δ_{31} and δ_{41}. The second sub-figure shows rotor speeds of the four synchronous generators. The third sub-figure shows the output power levels from the four synchronous generators.

Figs. 13 and 14 show the dynamic responses of the synchronous generators and the wind generator, with the auxiliary
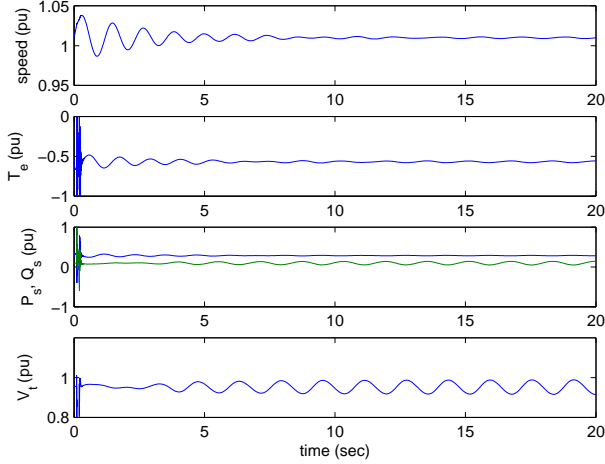
Fig. 12. Wind turbine generation dynamic responses with no supplementary damping control. The first sub-figure shows the speed of DFIG rotor. The second sub-figure shows the mechanical torque. The third sub-figure shows the output P and Q of the DFIG. Note that at steady state the curve P is above curve Q. The fourth sub-figure shows the terminal voltage magnitude of the DFIG.

damping control added for active power modulation. It is found that active power modulation can effectively enhance the damping of the inter-area oscillation.
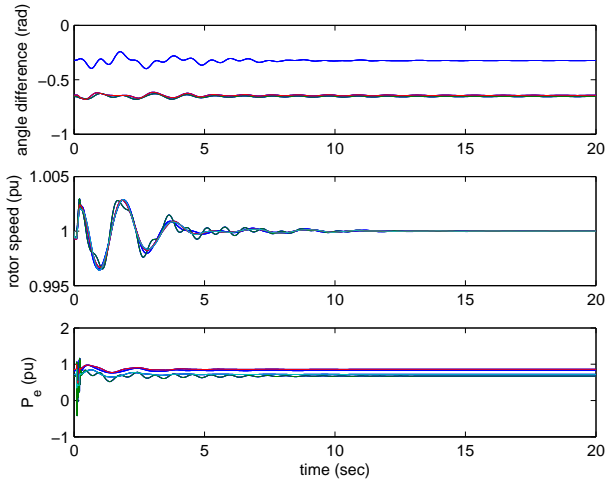

Fig. 13. Synchronous generator dynamic responses with active power modulation damping control. The first sub-figure shows relative rotor angles δ_{21}, δ_{31} and δ_{41}. The second sub-figure shows rotor speeds of the four synchronous generators. The third sub-figure shows the output power levels from the four synchronous generators.

Figs. 15 and 16 show the dynamic responses of the synchronous generators and the wind generator, with the auxiliary damping control added for reactive power modulation. It is found that reactive power modulation can also effectively enhance the damping of the inter-area oscillation.

A comparison of active and reactive power modulation will be done as follows. First of all, the dynamic responses of the rotor angles (synchronous generators) are plotted together for the three scenarios: 1) with no damping control, 2) with active power modulation, and 3) with reactive power modulation.
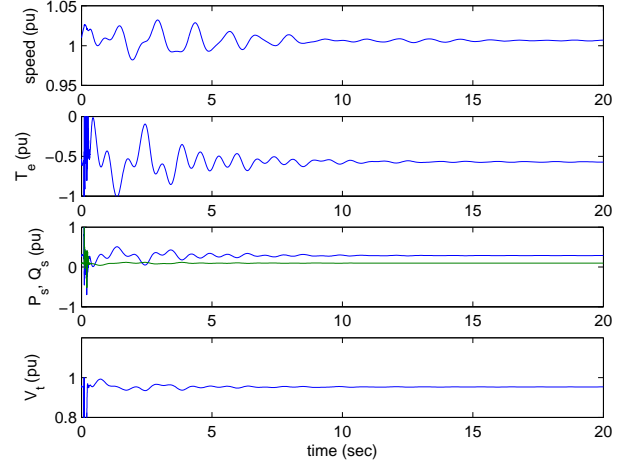

Fig. 14. Wind turbine generator dynamic responses with active power modulation damping control. The first sub-figure shows the speed of DFIG rotor. The second sub-figure shows the mechanical torque. The third sub-figure shows the output P and Q of the DFIG. Note that the curve P is above curve Q. The fourth sub-figure shows the terminal voltage magnitude of the DFIG.
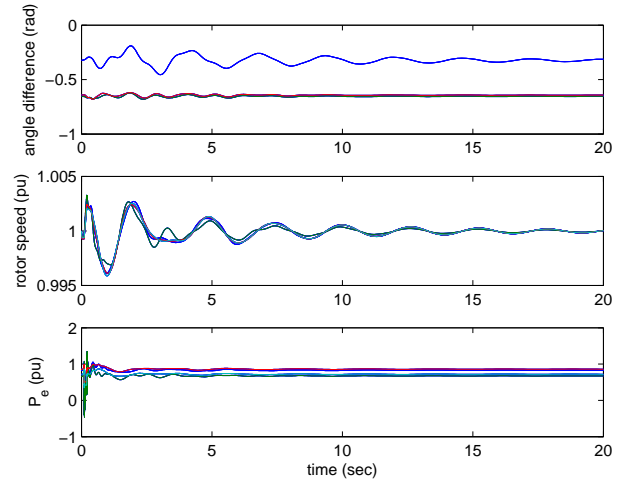

Fig. 15. Synchronous generator dynamic responses with reactive power modulation damping control. The first sub-figure shows relative rotor angles δ_{21}, δ_{31} and δ_{41}. The second sub-figure shows rotor speeds of the four synchronous generators. The third sub-figure shows the output power levels from the four synchronous generators.

The plots are shown in Fig. 17 where dashed lines correspond to the first scenario and the solid lines correspond to the second and third scenarios. From the plots, we can observe the effectiveness of the damping controllers in damping out the 0.7 Hz inter-area oscillation. Compared to the unstable original case, the system becomes stable with the addition of a supplementary control loop. The enhanced stability can further help to improve transfer capability and move more wind power to the market.

The dynamic responses of the electromagnetic torque of the wind generator are shown in Fig. 18 where dashed lines correspond to the first scenario and the solid lines correspond to the second and third scenarios. From Fig. 18, we can observe more oscillations in the torque when active power
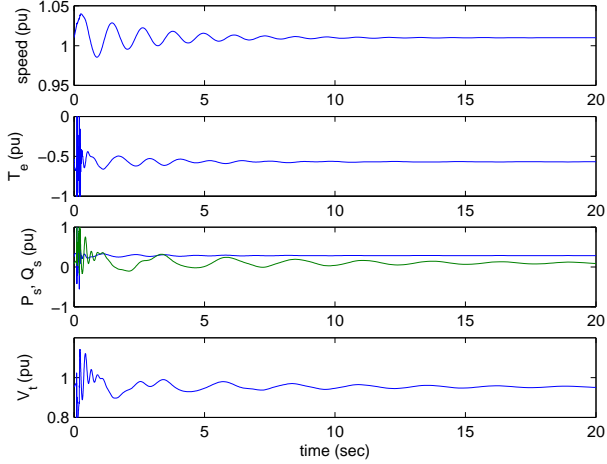
Fig. 16. Wind turbine generator dynamic responses with reactive power modulation damping. The first sub-figure shows the speed of DFIG rotor. The second sub-figure shows the mechanical torque. The third sub-figure shows the output P and Q of the DFIG. Note that the curve P is above curve Q. The fourth sub-figure shows the terminal voltage magnitude of the DFIG.
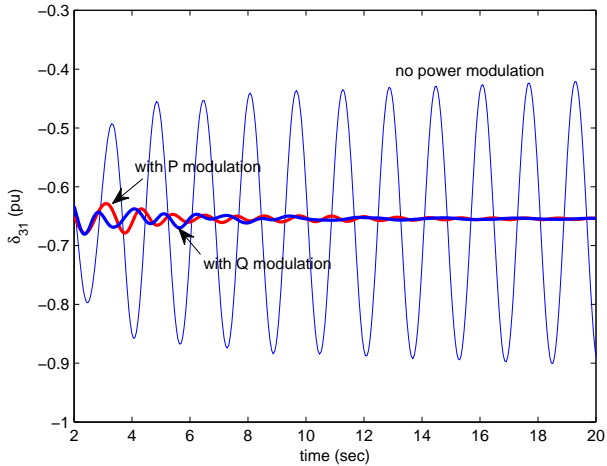

Fig. 17. Dynamic responses of relative rotor angle δ_{31}.

Fig. 18. Dynamic responses of electromagnetic torque.

Fig. 19. Dynamic responses of the terminal voltage of the wind farm.

modulation is applied. The waveform of T_e suggests that there are different oscillation modes. From the analysis in Section V, we find that the shaft mode becomes obvious due to decreased damping. In the case of reactive power modulation, the dynamic response of T_e is better than that of the case without any power modulation. This is because the reactive power modulation will not excite the shaft mode.

The dynamic responses of the terminal voltage of the wind farm are plotted in Fig. 19. In the original scenario, V_t has sustained oscillations due to an unstable inter-area oscillation mode. In the active power modulation scenario, V_t can be kept steady at its set value. Reactive power modulation apparently influences the terminal voltage and hence we can observe oscillations in its waveform initially. As time goes, oscillations in the terminal voltage will damp out.

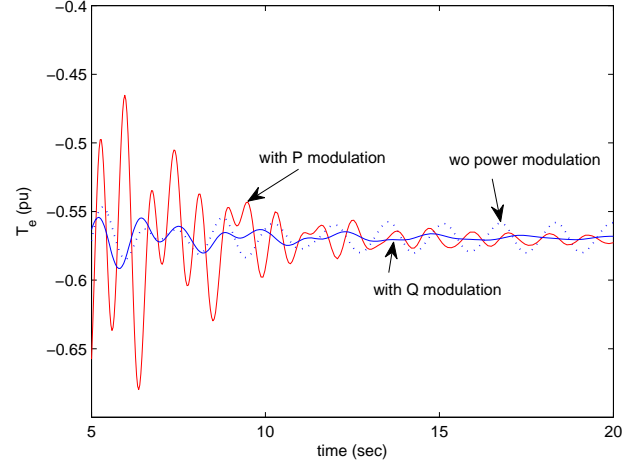In summary, to avoid the interaction between the active power modulation and the torsional oscillations, reactive power modulation can be sought as this paper has shown. The disadvantage of reactive power modulation is the introduction of oscillations in terminal voltage profile.

Another way to avoid the interaction is to design the active power modulation based controller with consideration of torsional dynamics. Parameters of the controllers will be chosen by trial and error or optimization to make sure that the damping of both the electric oscillation mode and the torsional mode can be improved. A recent paper in IEEE Trans. Power Systems [21] has practiced control design based on both eigenvalues and partial eigenstructure to achieve such goals.

VI. CONCLUSION

In this paper two methods for damping the interarea oscillations in a DFIG-based wind farm, namely, active and reactive power modulation, are compared for their effectiveness in damping and their interaction with wind turbine's shaft dynamics. A test system is built in Matlab/Simulink and a linear system analysis is carried out. Both methods are effective in

the oscillations. The major finding of the paper is that the the damping of the shaft mode decreases due to active power modulation in wind farms while reactive power modulation is immune to such risk.

APPENDIX

The parameters of synchronous generator are listed in Table I, and the parameters of DFIG are given in Table II.

TABLE I
PARAMETERS OF SYNCHRONOUS GENERATOR

r_s (pu)	0.003	X_{ls} (pu)	0.19
X_q (pu)	1.8	X_d (pu)	1.8
r'_{kq1} (pu)	0.00178	r'_{fd} (pu)	0.000929
X'_{lkq1} (pu)	0.8125	X'_{lfd} (pu)	0.11414
r'_{kq2} (pu)	0.00841	r'_{kd} (pu)	0.01334
X'_{lkq2} (pu)	0.0939	X'_{lkd} (pu)	0.08125

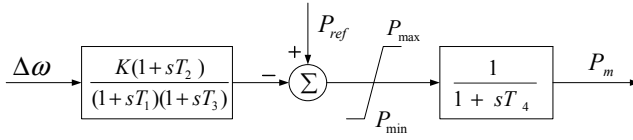The governor block is shown in Fig 20 and the parameters are shown in Table II.

Fig. 20. Governor model of Synchronous Generator.

TABLE II
PARAMETERS OF SYNCHRONOUS GENERATOR GOVERNOR

K	25
T_1 (s)	0.2
T_2 (s)	0.1
T_3 (s)	0.3
T_4 (pu)	0.01

A PSS consists of three blocks as shown in Fig. 21: a gain block, a signal washout block, and a phase compensation block [22]. The PSS transfer function is expressed as
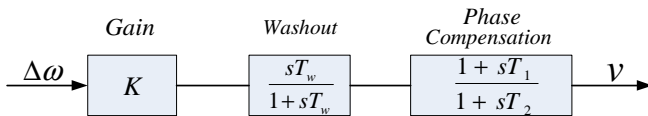

Fig. 21. Transfer function of PSS.

$$H(s) = 10 \frac{10s}{1 + 10s} \frac{1 + sT_1}{1 + sT_2}. \tag{9}$$

where $T_1 = 0.078$ and $T_2 = 0.21$.

TABLE III
PARAMETERS OF THE DFIG

r_s (pu)	0.00488
r_r (pu)	0.00549
X_{ls} (pu)	0.09231
X_{lr} (pu)	0.09955
X_M (pu)	3.95279
H (pu))	3.5

TABLE IV
PARAMETERS OF THE SHAFT SYSTEM OF DFIG

H_t (s)	0.09955
H_g (s)	3.95279
D_t (pu)	0
D_g (pu)	0
D_{tg} (pu)	0.09231
K_{tg} (pu)	0.22

REFERENCES

[1] Z. Miao, L. Fan, D. Osborn, and S. Yuvarajan, "Control of DFIG-based wind generation to improve interarea oscillation damping," *IEEE Trans. Energy Convers.*, vol. 24, no. 2, pp. 415–422, Jun. 2009.

[2] R. Johnson, N. Klemm, H. D. Laneuville, S. Koetschau, and G. Wild, "Power modulation of Sidney HVDC scheme. i. RAS control concept, realization and field tests," *IEEE Trans. Power Del.*, vol. 4, no. 4, pp. 2145–2152, Oct. 1989.

[3] M. Bahrman, E. Larsen, R. Piwko, and H. Patel, "Experience with HVDC - turbine generator torsional interaction at squre butte," *IEEE PAS*, vol. 99, pp. 966–975, May/June 1980.

[4] N. Mithulananthan, C. Canizares, J. Reeve, and G. Rogers, "Comparison of PSS, SVC, and STATCOM controllers for damping power system oscillations," *IEEE Trans. Power Syst.*, vol. 18, no. 2, pp. 786–792, May 2003.

[5] F. M. Hughes, O. Anaya-Lara, N. Jenkins, and G. Strbac, "A power system stabilizer for DFIG-based wind generation," *IEEE Trans. Power Syst.*, vol. 21, pp. 763–772, May 2006.

[6] Y. Mishra, S. Mishra, M. Tripathy, N. Senroy, and Z. Dong, "Improving stability of a DFIG-based wind power system with tuned damping controller," *IEEE Trans. Energy Convers.*, vol. 24, no. 3, pp. 650–660, Sep. 2009.

[7] G. Tsourakis, B. M. Nomikos, and C. D. Vournas, "Contribution of doubly fed wind generators to oscillation damping," *IEEE Trans. Energy Convers.*, vol. 24, no. 3, pp. 783–791, Sep. 2009.

[8] O. Anaya-Lara, F. M. Hughes, N. Jenkins, and G. Strbac, "Contribution of DFIG-based wind farms to power system short-term frequency regulation," *IEE Proc.-Gener. Transm. Distrib.*, vol. 153, pp. 164–170, March 2006.

[9] A. Tapia, G. Tapia, J. X. Ostolaza, and J. R. Saenz, "Modeling and control of a wind turbine driven doubly fed induction generator," *IEEE Trans. Energy Convers.*, vol. 18, pp. 194–204, Jun 2003.

[10] S. Muller, M. Deicke, and R. W. D. Doncker, "Doubly fed induction generator systems for wind turbine," *IEEE Ind. Appl. Mag.*, pp. 26–33, May/June 2002.

[11] R. Piwko, N. Miller, J. Sanchez-Gasca, X. Yuan, R. Dai, and J. Lyons, "Integrating large wind farms into weak power grids with long transmission lines," in *IEEE/PES Transmission and Distribution Conference & Exhibition: Asia and Pacific*, Dalian, China, 2005.

[12] H. Yin, L. Fan, and Z. Miao, "Reactive power modulation for inter-area oscillation damping of DFIG-based wind generation," in *IEEE Power & Energy Society General Meeting*, Minneapolis, US, Jul. 2010.

[13] R. Fernandez, R. Mantz, and P. Battaiotto, "Contribution of wind farms to the network stability," in *IEEE Power & Energy Society (PES) General Meeting*, Jun. 2006.

[14] F. Mei and B. C. Pal, "Modelling of dobuly-fed induction generator for power system stability study," in *IEEE Power & Energy General Meeting*, Jul. 2008.

[15] Z. Miao and L. Fan, "The art of modeling high-order induction generators in wind generation applications," *Simulation and Modelling Practice and Theory*, vol. 16, pp. 1239–1253, Oct. 2008.

[16] H. Li and Z. Chen, "Transient stability analysis of wind turbines with induction generators considering blades and shaft flexibility," in *the 33rd Annual Conference of the IEEE Industrial Electronics Society (IECON)*, Taipei, Taiwan, Nov. 2007.

[17] W. Qiao, W. Zhou, J. Aller, and R. Harley, "Wind speed estimation based sensorless output maximization control for a wind turbine driving

a DFIG," *IEEE Trans. Power Electron.*, vol. 23, no. 3, pp. 1156–1169, May 2008.

[18] P. Krause, *Analysis of Electric Machinery*. New York: McGraw-Hill, 1986.

[19] L. Fan, A. Feliachi, and K. Schoder, "Selection and design of a TCSC control signal in damping power system inter-area oscillations for multiple operating conditions," *Electric Power Systems Research*, vol. 62, no. 2, pp. 127–137, Jun. 2002.

[20] E. Larsen, J. Sanchez-Gasca, and J. Chow, "Concepts for design of FACTS controllers to damp power swings," *IEEE Trans. Power Syst.*, vol. 10, no. 2, pp. 948–956, May 1995.

[21] N. Kshatriya, U. D. Annakkage, F. Hughes, and A. M. Gole, "Optimized partial eigenstructure assignment-based design of a combined PSS and active damping controller for a DFIG," *IEEE Trans. Power Syst.*, vol. 25, no. 2, pp. 866–876, May 2010.

[22] P. Kundur, *Power system stability and control*. McGraw Hill, 1994.

Lingling Fan (S'99-M'02-SM'08) received the B.S. and M.S. degrees in electrical engineering from Southeast University, Nanjing, China, in 1994 and 1997, respectively, and the Ph.D. degree in electrical engineering from West Virginia University, Morgantown, WV, in 2001.

She is currently an Assistant Professor in the Department of Electrical Engineering, University of South Florida (USF). Before joining USF, she was with North Dakota State University (2007-2009) and Midwest ISO (2001-2007). Her research interests include modeling and control of energy systems, large-scale power systems planning and operation.

Haiping Yin is a Ph.D. student in Department of Electrical Engineering at University of South Florida. She obtained her Master and Bachelor degrees in Electrical Engineering from Nanjing Normal University, Nanjing China in 2005 and 2008.

Zhixin Miao (S'00-M'03-SM'09) received the B.S. degree from Huazhong University of Science & Technology, Wuhan, China, in 1992, the M.S. degree from the Graduate School of Nanjing Automation Research Institute in 1997, and the Ph.D. degree in electrical engineering from West Virginia University, Morgantown, in 2002.

He is currently with the University of South Florida (USF), Tampa, FL. Prior to joining USF in 2009, he was with the transmission asset management department in Midwest ISO, St. Paul, Minnesota from 2002 to 2009. His research interests include power system stability, microgrids, and renewable energy.